arXiv:cond-mat/9605004v1 1 May 1996

Rescaling Relations between Two- and Three-Dimensional Local Porosity Distributions for Natural and Artificial Porous Media

B. Virgin[a], E. Haslund[a] and R. Hilfer[a,b,c]

[a]Department of Physics, University of Oslo, 0316 Oslo, Norway
[b]Institut für Physik, Universität Mainz, W-55099 Mainz, Germany
[c]ICA-1, Universität Stuttgart, Pfaffenwaldring 27, 70569 Stuttgart, Germany

Abstract

Local porosity distributions for a three-dimensional porous medium and local porosity distributions for a two-dimensional plane-section through the medium are generally different. However, for homogeneous and isotropic media having finite correlation-lengths, a good degree of correspondence between the two sets of local porosity distributions can be obtained by rescaling lengths, and the mapping associating corresponding distributions can be found from two-dimensional observations alone. The agreement between associated distributions is good as long as the linear extent of the measurement cells involved is somewhat larger than the correlation length, and it improves as the linear extent increases. A simple application of the central limit theorem shows that there must be a correspondence in the limit of very large measurement cells, because the distributions from both sets approach normal distributions. A normal distribution has two independent parameters: the mean and the variance. If the sample is large enough, LPDs from both sets will have the same mean. Therefore corresponding distributions are found by matching variances of two- and three-dimensional local porosity distributions. The variance can be independently determined from correlation functions. Equating

variances leads to a scaling relation for lengths in this limit. Three particular systems are examined in order to show that this scaling behavior persists at smaller length-scales.

1 Introduction

The study of porous and heterogeneous media is scattered throughout many fields of science, including mathematics, solid state physics and chemistry, materials science, geology, hydrology, environmental technology, petroleum engineering and separation technology. The central problem is the specification of the random microstructure, which is needed to predict macroscopic physical properties (see [1][2][3][4][5] for overviews).

A complete specification of the random microstructure is both impractical and unnecessary. It is therefore important to have a general statistical description of the microstructure available. Such a description should meet four criteria: it should be well-defined in terms of geometrical quantities, it should involve only experimentally accessible parameters, it should be of economical size and it should be usable in exact or approximate solutions of the underlying equations of motion. Currently there are only two statistical methodologies available which fulfill all four requirements; these are correlation functions [6][7][8][9][10][11][12][13][14][15] and local geometry distributions [16][18][17][19][3].

The recently developed local geometry distributions are a functional generalization of the correlation-function approach[3]. The aim of the present paper is to increase the practical applicability of local geometry distributions. Interest in these distributions arises from their potential use in distinguishing between different microstructures[17]. Increasing their practical applicability is particularly important because local geometry distributions can be used in mean field theory calculations of the dielectric and transport properties of various porous media, for instance porous rock filled with brine[16][18]. Preliminary comparisons of the theory with experimental results have already been carried out, and show good agreement[19][20].

Two main objectives will be pursued in the present paper. First, we show the feasibility of obtaining three-dimensional local porosity distributions(LPDs), by presenting data from a real sandstone specimen. Second, we show to what extent three-dimensional LPDs can be obtained from purely two-dimensional observations. The dependence of LPDs upon the dimensionality of the system is a consequence of their dependence on a measurement cell or observation region over which geometric observables, such as porosity, are averaged. The possibility of extracting three-dimensional distributions from two-dimensional data arises from limit theorems which guarantee that

the asymptotic LPDs become independent of the shape of the measurement cell[3].

We begin our discussion with a definition of LPDs. Next we present a simple argument based on the central limit theorem showing that for large measurement cells, three-dimensional LPDs can be mapped onto two-dimensional LPDs by a simple rescaling of lengths. Then, we show that this mapping becomes exact for the percolation model. Subsequently, we analyse the overlapping sphere (or continuum percolation) model, where the mapping holds only asymptotically. Finally we present the first measurement of three-dimensional LPDs. These are obtained from the pore-space reconstruction of a real sandstone specimen.

The main result of our investigation is the fact that the mapping between two- and three-dimensional LPDs can be determined from purely two-dimensional observations if the medium is homogeneous and isotropic. For general anisotropic media however, the family of three-dimensional LPDs can only be determined from a three-dimensional measurement.

2 Basic Concepts and an Expression for Variance

The discretized porous medium is considered to occupy a set $\mathbf{S} \subset \mathbf{Z}^d$, where $\mathbf{Z}$ is the set of integers. Pore-space is denoted by $\mathbf{P}$, where $\mathbf{P} \subset \mathbf{S}$. Considering for simplicity only two-component media, we define matrix-space $\mathbf{M}$ as the complement of $\mathbf{P}$ in $\mathbf{S}$, $\mathbf{M} = \mathbf{S} - \mathbf{P}$. The characteristic function of a set $\mathbf{A}$ is

$$\chi_{\mathbf{A}}(\mathbf{r}) = \begin{cases} 1, & \mathbf{r} \in \mathbf{A} \\ 0, & \text{otherwise} \end{cases}$$

where $\mathbf{r} \in \mathbf{Z}^d$. To describe the state of each point in the system, we label each point in $\mathbf{S}$ with an index i and define the random variables

$$X_i \equiv X(\mathbf{r_i}) = \chi_{\mathbf{P}}(\mathbf{r_i})$$

A specific geometry is then specified by the N-tuple

$$g = (X_1, \ldots, X_N), \qquad N = |\mathbf{S}|$$

where $|\mathbf{S}|$ is the number of elements in $\mathbf{S}$.

The probability space for the system is the triple $(\mathbf{G}, \mathcal{E}, P)$. $\mathbf{G}$ is the sample space consisting of all possible geometries g. The event space $\mathcal{E}$ is a Boolean algebra of subsets of $\mathbf{G}$. The probability P of finding a geometry[1] g is a finitely additive non-negative set function defined on $\mathcal{E}$, such that $P(\emptyset) = 0$ and $P(\mathbf{G}) = 1$. A stochastic medium is homogenous if P is invariant under translations. Isotropy is defined analogously as invariance under rotations. The expectation value of a random variable $f(g)$ is

$$\langle f(g) \rangle = \sum_{g \in \mathbf{G}} f(g) P(g)$$

and in the following, we will use the notation

$$\begin{aligned} S_n(\mathbf{r}_1, \ldots, \mathbf{r}_n) &= \langle \prod_{i=1}^{n} \chi_{\mathbf{P}}(\mathbf{r}_i) \rangle \\ C_n(\mathbf{r}_1, \ldots, \mathbf{r}_n) &= \langle \prod_{i=1}^{n} \chi_{\mathbf{P}}(\mathbf{r}_i) - \langle \chi_{\mathbf{P}}(\mathbf{r}_i) \rangle \rangle \end{aligned}$$

for the moment functions $S_n(\mathbf{r}_1, \ldots, \mathbf{r}_n)$ and cumulant functions $C_n(\mathbf{r}_1, \ldots, \mathbf{r}_n)$ of order n. For homogeneous media, $S_1(\mathbf{r}) = \langle \phi \rangle$ is the expected bulk porosity.

Given a measurement cell denoted as $\mathbf{K}$ ($\mathbf{K} \subset \mathbf{S}$), we define the local porosity of $\mathbf{K}$ as the random variable

$$\phi(\mathbf{K}) = \frac{|\mathbf{P} \cap \mathbf{K}|}{|\mathbf{K}|} = \frac{1}{|\mathbf{K}|} \sum_{\mathbf{r} \in \mathbf{Z}^d} \chi_{\mathbf{P}}(\mathbf{r}) \chi_{\mathbf{K}}(\mathbf{r})$$

The local porosity distribution(LPD)[16] for $\mathbf{K}$ can be defined as[3]

$$\mu(\phi; \mathbf{K}) = \langle \delta(\phi - \phi(\mathbf{K})) \rangle$$

where $\delta(\phi - \phi(\mathbf{K}))$ is the Dirac delta function, and the first moment of this LPD is

$$\overline{\phi\,(\mathbf{K})} = \int_0^1 \phi\, \mu(\phi; \mathbf{K})\, d\phi$$

[1]Strictly speaking, P is defined on sets of geometries $\mathbf{E} \in \mathcal{E}$. However, we assume that $\{g\} \in \mathcal{E}$ for all $g \in \mathbf{G}$.

Using the definition of μ, and changing the order of summation gives

$$\overline{\phi\,(\mathbf{K})} = \sum_{g\in\mathbf{G}} \left(\int_0^1 \phi\,\delta(\phi - \phi(\mathbf{K}))\,d\phi \right) P(g) = \sum_g \phi(\mathbf{K}) P(g) = \langle \phi(\mathbf{K}) \rangle$$

$$= \left\langle \frac{1}{|\mathbf{K}|} \sum_{\mathbf{r}\in\mathbf{Z^d}} \chi_{\mathbf{P}}(\mathbf{r})\chi_{\mathbf{K}}(\mathbf{r}) \right\rangle = \frac{1}{|\mathbf{K}|} \sum_{\mathbf{r}} \langle \chi_{\mathbf{P}}(\mathbf{r}) \rangle \chi_{\mathbf{K}}(\mathbf{r})$$

where we have also used the definition of $\phi(\mathbf{K})$. Thus, we obtain the expression

$$\overline{\phi\,(\mathbf{K})} = \int_0^1 \phi\,\mu(\phi;\mathbf{K})\,d\phi = \langle \phi(\mathbf{K}) \rangle = \frac{1}{|\mathbf{K}|} \sum_{\mathbf{r}} S_1(\mathbf{r})\chi_{\mathbf{K}}(\mathbf{r}) \tag{1}$$

For homogeneous media, $S_1 = \langle \phi \rangle$, the bulk porosity, so that $\overline{\phi\,(\mathbf{K})} = \langle \phi \rangle$. Similarly, we can show that the local porosity variance $var[\phi\,(\mathbf{K})] = \int_0^1 \left(\phi - \overline{\phi\,(\mathbf{K})} \right)^2 \mu(\phi;\mathbf{K})\,d\phi$ is given by

$$var\,[\phi(\mathbf{K})] = \frac{1}{|\mathbf{K}|^{\mathbf{2}}} \sum_{\mathbf{r},\mathbf{r}'\in\mathbf{Z}^d} C_2(\mathbf{r},\mathbf{r}')\chi_{\mathbf{K}}(\mathbf{r})\chi_{\mathbf{K}}(\mathbf{r}') \tag{2}$$

If the medium is homogeneous we can perform one of the sums. In this case $C_2(\mathbf{r},\mathbf{r}') = C_2(\mathbf{0},\mathbf{r}'-\mathbf{r})$. Defining $\mathbf{y} = \mathbf{r}' - \mathbf{r}$, and using the fact that $\chi_{\mathbf{K}}(\mathbf{r}+\mathbf{y}) = \chi_{\mathbf{K}-\mathbf{y}}(\mathbf{r})$, where $\mathbf{K}-\mathbf{y}$ is the set $\mathbf{K}$ translated by the vector $-\mathbf{y}$, we obtain

$$var\,[\phi(\mathbf{K})] = \sum_{\mathbf{y}\in\mathbf{Z}^d} \frac{|\mathbf{K}\cap(\mathbf{K}-\mathbf{y})|}{|\mathbf{K}|^{\mathbf{2}}} C_2(\mathbf{0},\mathbf{y}) \tag{3}$$

Note that the variance $var[\phi\,(\mathbf{K})]$ is simply related to the granularity concept which is used for photographic materials[21]. The relations above are applicable to infinitely large realizations of homogeneous stochastic media.

3 The Central Limit Theorem and Scaling

Consider again the class of homogeneous media in which spatial correlations of the random geometry decay with a finite correlation-length ξ. For such systems, we can apply the central limit theorem to measurements of local porsity

for very large measurement cells. To do this, we partition a d-dimensional hypercubic measurement cell $\mathbf{K}$ of side L into $n = (L/a)^d$ hypercubic subcells $\{\mathbf{K}_i\}$, $i = 1, 2, \ldots, n$, of side a so that

$$\mathbf{K} = \bigcup_{i=1}^{n} \mathbf{K}_i, \qquad \mathbf{K}_i \cap \mathbf{K}_j = \emptyset \quad \text{for} \quad i \neq j$$

and rewrite $\phi(\mathbf{K})$ as the average

$$\phi(\mathbf{K}) = \frac{1}{n} \sum_i \phi(\mathbf{K}_i)$$

over all the subcell porosities $\phi(\mathbf{K}_i)$. If we choose L and a such that $\xi \ll a \ll L$, then $n \gg 1$, and the central limit theorem becomes applicable, because the $\phi(\mathbf{K}_i)$ are weakly correlated random variables. The central limit theorem ensures the existence of a number σ such that

$$\mu(\phi; \mathbf{K}) \simeq \frac{(L/a)^{d/2}}{\sqrt{2\pi}\sigma} \exp\left[-\frac{(\phi - \overline{\phi})^2 (L/a)^d}{2\sigma^2} \right]$$

were the accuracy of the approximate equality improves as L/a increases. In the limit $L/a \to \infty$ subject to $a \gg \xi$, one has $\mu \to \delta(\phi - \overline{\phi})$, independent of dimension and independent of $\mathbf{K}$. Hence, for L/a sufficiently large but still finite, the form of $\mu(\phi; \mathbf{K})$ depends only on the bulk porosity $\overline{\phi}$ and the variance $var[\phi(\mathbf{K})] = \sigma^2/(L/a)^d$, but not on the shape of $\mathbf{K}$. If the medium is also isotropic, then a sufficient condition for the equality of two such limiting distributions for d and d'-dimensional measurement cells in the same medium is thus

$$\left(\frac{L'}{a'} \right) = \left(\frac{\sigma'}{\sigma} \right)^{2/d'} \left(\frac{L}{a} \right)^{d/d'} \tag{4}$$

because $\overline{\phi}$ will be the same in both cases.

Thus we find that for homogeneous isotropic systems with finite correlation-length, two- and three-dimensional LPDs for large L are simply related by a rescaling of lengths. We now examine the site percolation model, for which the scaling relation is exact.

4 The Percolation Model

In the site percolation model, each lattice site has a probability $\langle\phi\rangle$ of being occupied and $(1 - \langle\phi\rangle)$ of being empty that is independent of the other sites. Therefore, if we consider occupied sites to be pore and empty sites as matrix, $\mu(\phi; \mathbf{K})$ depends only on $\langle\phi\rangle$ and $|\mathbf{K}|$, and is given by the binomial distribution. If the underlying lattice is hypercubic, then the LPD for a d-dimensional hypercubic measurement cell $\mathbf{K}$ of side L is

$$\mu(\phi_i; \mathbf{K}) = \frac{L^d!}{[L^d\,\phi_i]!\ [L^d\ (1-\phi_i)]!}\ \langle\phi\rangle^{\,L^d\phi_i}\,(1-\langle\phi\rangle)^{\,L^d(1-\phi_i)}$$

where $\phi_i = i/L^d$ and $i = 0, 1, \ldots, L^d$. Measurement cells consisting of the same number of points must have identical LPDs. Therefore, if $\mathbf{K}^{'}$ is a $d^{'}$-dimensional measurement cell of side $L^{'}$

$$\mu(\phi_i; \mathbf{K}^{'}) = \mu(\phi_i; \mathbf{K}) \ \text{ if } \ L^{'d^{'}} = L^d$$

The scaling relation

$$L^{'} = L^{d/d^{'}} \tag{5}$$

is not solvable in $\mathbf{Z}$ for all L, $L^{'}$. Nevertheless, there exist infinitely many solutions, since each positive integer i yields the solution $L^{'} = i^d$ and $L = i^{d^{'}}$ Therefore, for the site percolation model, two- and three-dimendional LPDs are, within the constraints imposed by the discrete nature of the model, simply related by a rescaling of lengths.

5 The Overlapping Sphere Model

An often useful grain model for porous media is obtained by randomly distributing overlapping spheres. The spheres represent grains of matrix material. A model configuration is typically created by randomly distributing point-centers with constant point-density in a given volume and attaching a sphere of radius r_0 to each point-center. The system analyzed below was obtained by randomly distributing 8000 point-centers in a volume of 256x256x256 voxels. A value of $r_0 = 9.45$ voxels has been used, and periodic boundary conditions have been implemented. The bulk porosity of the overlapping sphere model is $\langle\phi\rangle = \exp\left[-\rho\frac{4}{3}\pi r_0^3\right]$, where ρ is the point-density.

The point density and sphere radius were chosen such that $\langle\phi\rangle = 0.1855$, matching the porosity of a real sandstone specimen discussed below. A plane-section showing the degree of discretization is displayed in Figure 1.

Three-dimensional LPDs for $L \in \{1, 2, \ldots, 64\}$ have been measured, and the resulting family of distributions is shown in Figures 2. Two-dimensional LPDs were obtained for $L^{'} \in \{1, 2, \ldots, 150\}$ by averaging the measured distributions for all cross-sections perpendicular to the z-axis. The results are displayed in Figure 3. To investigate the degree of correspondence between two- and three-dimensional LPDs we calculate the quantity

$$\Delta(L, L^{'}) = \int_0^1 \mid \mu_{3d}(\phi; L) - \mu_{2d}(\phi; L^{'}) \mid d\phi$$

as a quantitative measure of the deviation between two distributions. For fixed L, we minimize $\Delta(L, L^{'})$ by varying $L^{'}$. The matched distributions selected by this criterion are shown in Figure 4 for a choice of $(L, L^{'})$-values indicated in the figure for each matching pair. The agreement between the matched two- and three-dimensional distributions is satisfactory. The agreement for large L stipulated by the central limit theorem improves with better system-statistics. This is seen from the matched LPDs shown in Figure 5, for a system of 64000 instead of 8000 spheres, having the same voxel-dimensions and bulk porosity. The poorer sphere-resolution of $r_0 = 4.73$ pixels makes this configuration less suitable for analyzing μ at smaller length-scales, so we shall not discuss this configuration further.

The matching of distributions based on $\Delta(L, L^{'})$ is shown as the solid line in Figure 6. Another matching of distributions is obtained from the criterion of equal variances established in section 3. The mapping $L^{'}(L)$ obtained from the equal-variance criterion is shown as the dashed curve in Figure 6. For lengths that are not too large relative to the size of the system, both criteria give more or less the same rescaling of lengths $L^{'}(L)$. Note, however, that the discretization can affect $L^{'}(L)$ at small L.

In practical applications, it is important to estimate the three-dimensional LPDs from observations on two-dimensional cross-sections alone. In the matching above, however, it was assumed that the three-dimensional LPDs are known. A way out of this dilemma is provided by equations (3) and (4). The agreement between the dashed and the solid lines in Figure 6 validates the matching criterion based solely on the variances expressed in equation (4). On the other hand, equation (3) allows us to estimate the variance from

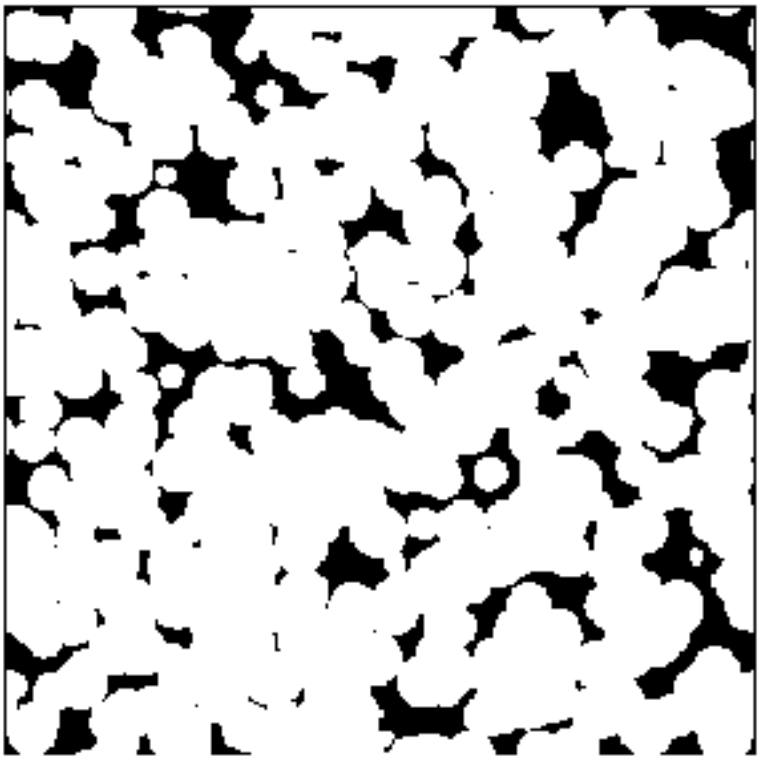

.

Figure 1: A digitized plane-section from a 256x256x256-voxel digitized configuration of overlapping spheres, consisting of 8000 randomly distributed spheres, all of radius $r_0 = 9.45$ voxels.

.

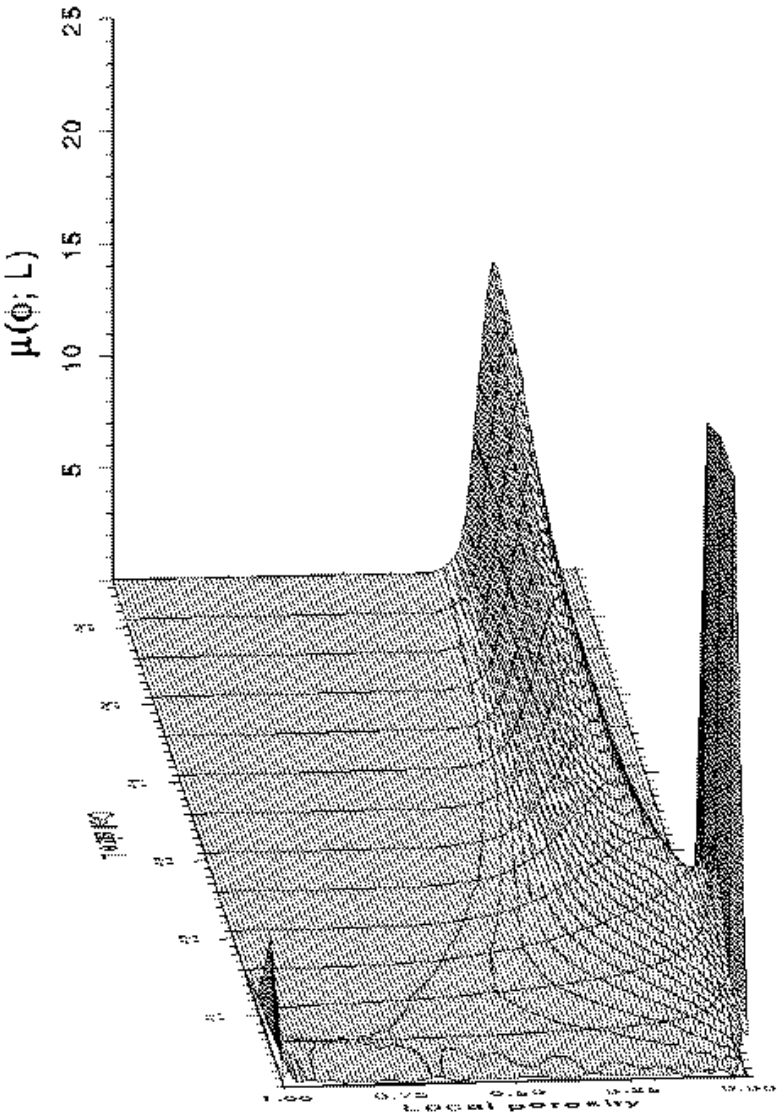

.

Figure 2: The family of three-dimensional LPDs $\mu_{3d}(\phi; L)$ for $L \in \{1, 2, \ldots, 64\}$ for the overlapping sphere model. Note that the position of the saddle-point is near $L = 18.9$, which is the correlation length for the system.

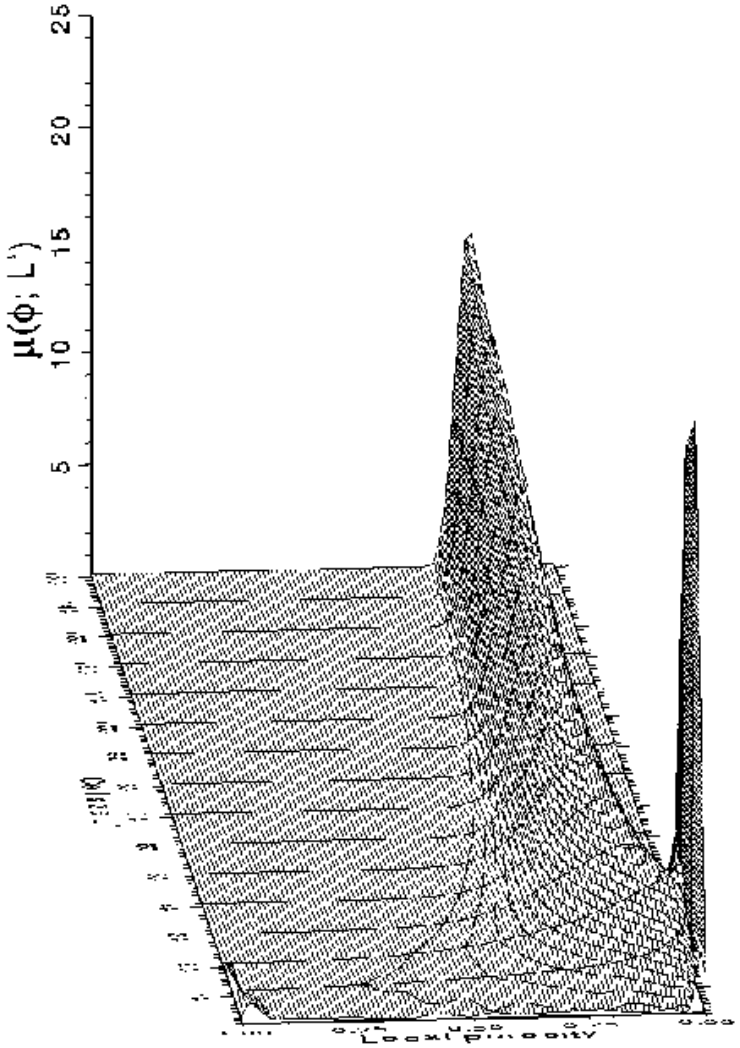

.

Figure 3: The family of two-dimensional LPDs $\mu_{2d}(\phi; L^{'})$ for $L^{'} \in \{1, 2, \ldots, 150\}$. Although this surface is not the same as the in the previous one, the previous surface can be approximately recreated from this one by rescaling the $L^{'}$ axis.

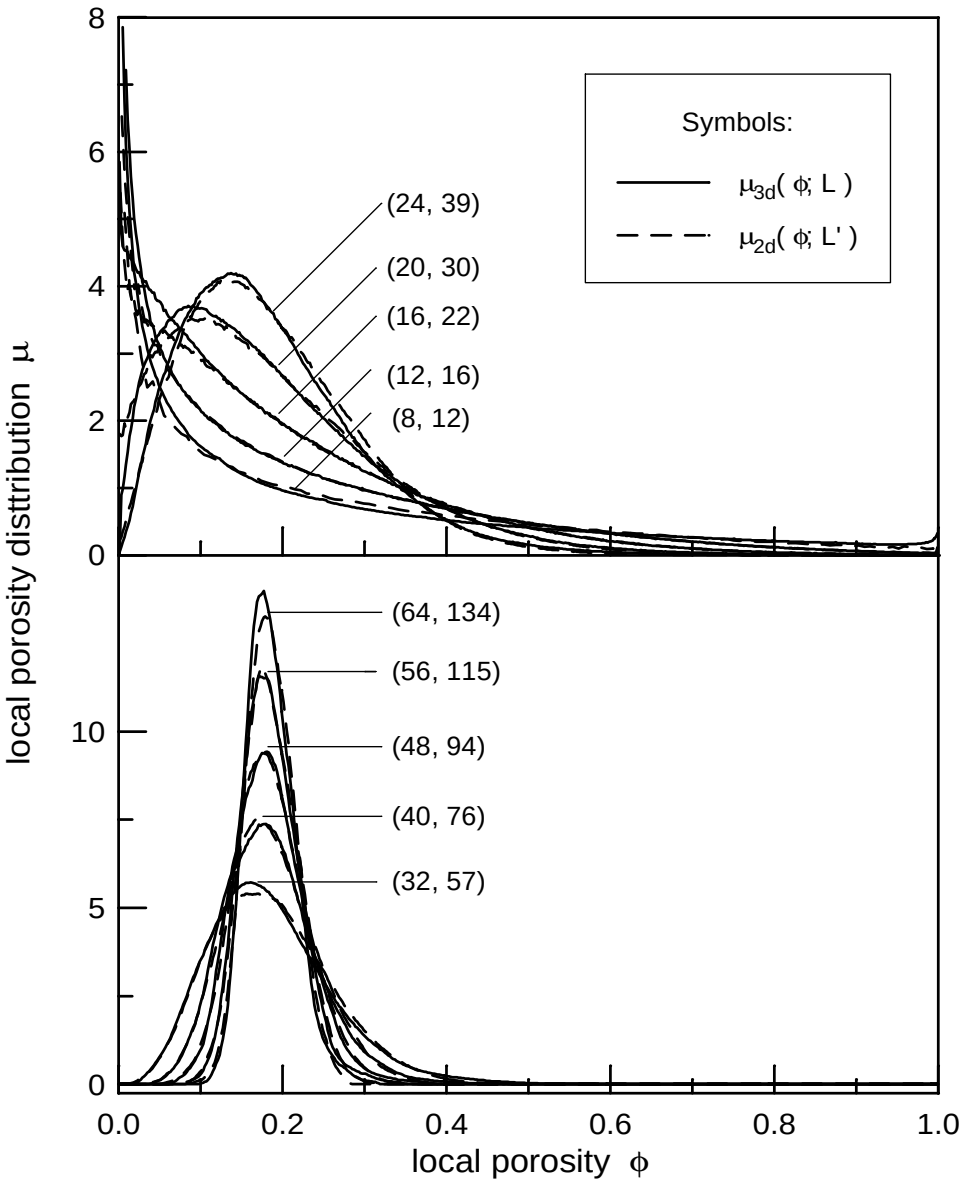

.

Figure 4: A selection of matching two- and three-dimensional LPDs from the mapping obtained by minimizing $\Delta(L, L^{'})$. Solid lines indicate three-dimensional LPDs and dashed lines show two-dimensional LPDs. The side-length of the measurement cells for matched LPDs are shown on the figure as $(L, L^{'})$-pairs.

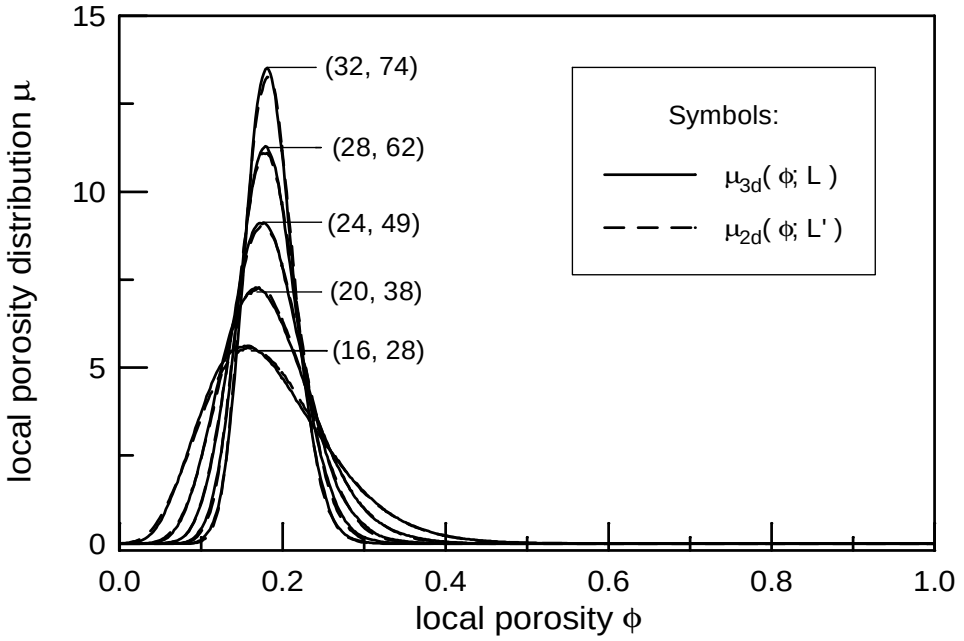

.

Figure 5: Selected $\Delta(L, L^{'})$-matched distributions, similar to those shown in the lower half of the previous figure, from an ensemble of 64000 spheres of $r_0 = 4.73$ voxels, within a volume of 256x256x256 voxels. The matching $(L, L^{'})$-pairs are indicated in the figure.

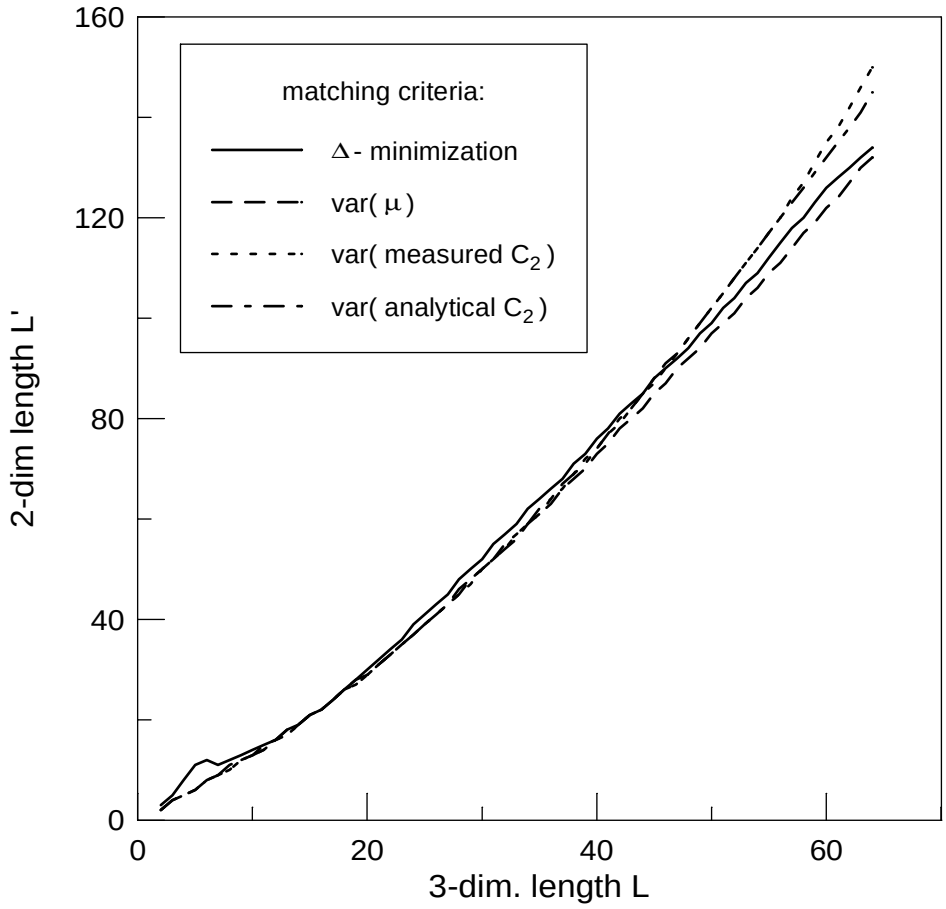

.

Figure 6: The scaling relation $L^{'}(L)$ associating two- and three-dimensional LPDs, as determined by four different criteria. The solid line is based on minimizing $\Delta(L, L^{'})$. The remaining curves are based on equating variances: the dashed curve is obtained from the actual distribution variances, the dotted curve and the dash-dotted curves are obtained from variances computed from (3) using measured and analytical values for C_2 respectively.

$C_2(\mathbf{0},\mathbf{r})$ measured on two-dimensional cross-sections as long as the system is isotropic. The results of such a matching procedure are shown as the dotted and the dash-dotted curves in Figure 6. The dotted curve uses a direct measurement of C_2 from two-dimensional sections, while the dash-dotted curve uses the exactly known analytical form of C_2. The direct measurement of C_2 uses the same series of planar-sections as the measurement of the two-dimensional LPDs; the correlation function is first calculated in each plane and subsequently averaged over all planes. The necessity to average over all planes, and the influence of discretization effects were recently discussed systematically[22]. The resulting averaged two-point correlation function

$$G(\mathbf{0},\mathbf{r}) = \frac{C_2(\mathbf{0},\mathbf{r})}{C_2(\mathbf{0},\mathbf{0})} = \frac{S_2(\mathbf{0},\mathbf{r}) - S_1(\mathbf{0})S_1(\mathbf{r})}{S_2(\mathbf{0},\mathbf{0}) - S_1(\mathbf{0})S_1(\mathbf{0})}$$

is shown in Figure 7. Because the model of overlapping spheres is homogeneous and isotropic $G(\mathbf{0},\mathbf{r}) = G(r)$. The exact analytical expression for $S_2(\mathbf{0},\mathbf{r})$ is given as

$$S_2(\mathbf{0},\mathbf{r}) = S_2(|\mathbf{r}|) = \exp\left[-\rho\left(\frac{\pi}{3}d^3 - V_3(\mathbf{B}(\mathbf{0},\frac{d}{2}) \cap \mathbf{B}(\mathbf{r},\frac{d}{2})\right)\right]$$

ρ is the density of point-centers, d is the sphere-diameter, $V_3(\mathbf{A})$ is the volume of the set $\mathbf{A}$ and $\mathbf{B}(\mathbf{r},c) = \{\mathbf{x} : |\mathbf{x}-\mathbf{r}| \leq c\}$ is the ball of radius c around $\mathbf{r}$. The exact $G(r)$ vanishes for $r \geq d$, and is shown as the dashed curve in Figure 7. Visible discrepencies between the measured and analytical curves are due to insufficient system-statistics.

The satisfactory agreement of the dotted and the dash-dotted curves in Figure 6 results from the isotropy of the overlapping sphere model. The isotropy condition $G(r) = G(\mathbf{r})$ guarantees knowledge of the full function $G(\mathbf{r})$ from a measurement along any ray. Knowledge of the full function is a prerequisite for calculating the three-dimensional variance from (3). Hence, the above precedure is not applicable for general anisotropic media.

To assess the relative reliability of our rescaling procedure for isotropic systems, we compare in Figure 8 the two- and three-dimensional variances computed from the exact and measured correlation functions $G(r)$ with those computed from the local porosity distribution $\mu(\phi;\mathbf{K})$. Solid lines are variances computed from $\mu(\phi;\mathbf{K})$, dashed lines are variances computed from the measured $G(r)$ and dotted lines are variances computed using the analytical

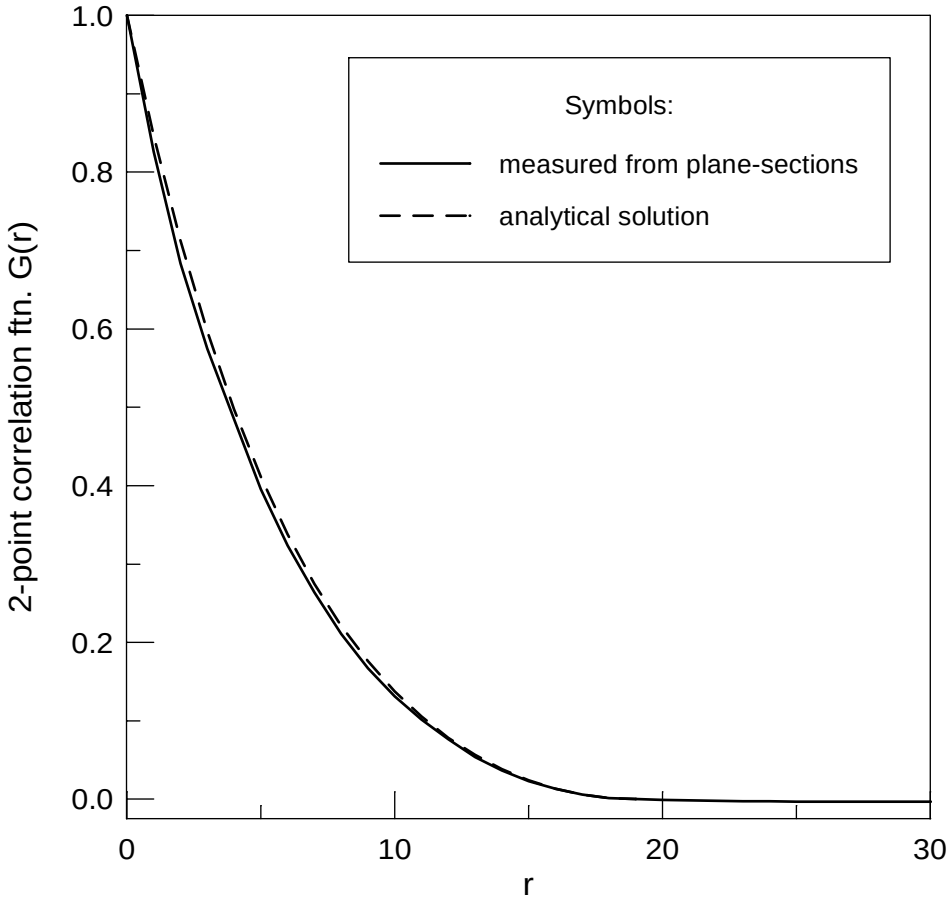

.

Figure 7: The 2-point correlation function G as a function of distance r. The solid curve shows measured values, while the dashed curve is the analytical result for an infinite sample.

$G(r)$. The overall agreement is satisfactory, given that the side length of the whole system is only 256 voxels.

6 A Sandstone specimen

In this section, we analyse experimental data. The three-dimensional pore-space for a specimen of Savonnier oolithic sandstone was reconstructed from serial thin sections[23]. The data-set consists of 99 binary images, each of 1904x1904 pixels, representing planar cross-sections through the medium. The distance between the planes of consecutive images is 10μm. This is also the pixel size. Each section was obtained by thresholding a digitized micrograph into a black and white image. The threshold value was chosen to match the experimentally-known bulk porosity of $\overline{\phi} = 0.1845$. Figure 9 shows part of a typical image measuring approximately 1 cm along each side. In Figure 10 we show a three-dimensional cubic subset with a side length of 1 mm, in which the pore-space is shown in black, the matrix is transparent and the pore-space boundary is gray.

Figure 10 shows that the pore-space is anisotropic. This is corroborated in Figure 11, where the correlation function $G_{\parallel}(r)$, measured in the plane of the thin sections is shown together with $G_{\perp}(r)$ measured in the direction normal to the thin sections. The anisotropy is at least partly caused by the misalignments of individual images and variations in lighting and thresholding during the reconstruction. The correlation function $G_{\parallel}(r)$ also shows the existence of large-scale heterogeneities. Given these imperfections we do not expect to be able to reconstruct the three-dimensional LPDs from two-dimensional information alone.

The family of three-dimensional LPDs is displayed in Figure 12. The family of two-dimensional LPDs is displayed in Figure 13. The three-dimensional distributions have been measured on a sub-system of 1881x1881x99 voxels for measurement cell sizes $L \in \{1, 2, \ldots, 96\}$. The bulk porosity of the sub-system is 0.1861. The results displayed in Figure 12 are, to our knowledge, the first measurements of three-dimensional LPDs on a natural rock sample. The two-dimensional LPDs shown for $L' \in \{1, 2, \ldots, 240\}$ were obtained, as before, by averaging the distributions for each plane.

Figure 14 shows the two- and three-dimensional variances computed directly from the distributions as solid lines. The dashed lines are variances ob-

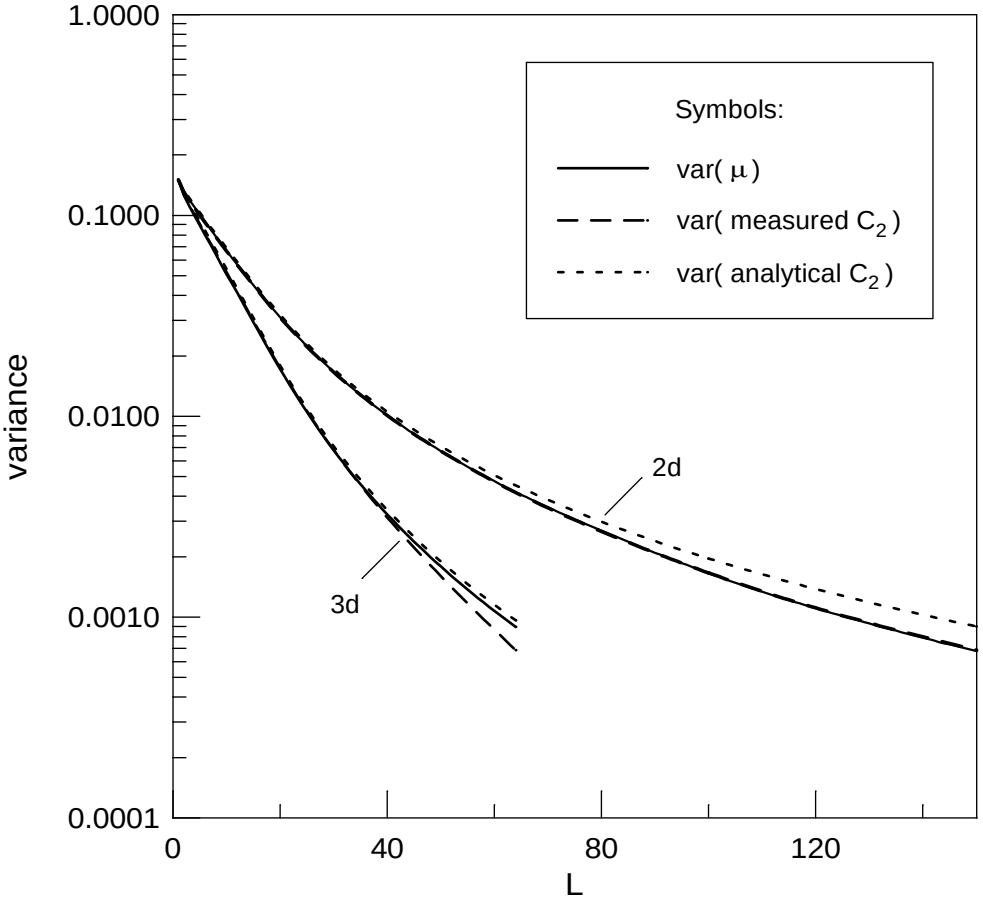

Figure 8: Three different determinations of variance for both two- and three-dimensional LPDs. The actual distribution-variances are the solid curves. The dashed and dash-dotted curves are computed from (3) using measured and analytical values for C_2 repectively.

.

Figure 9: Part of a typical planar-section through the Savonnier oolithic sandstone. The side-length of the image is ≈ 1 cm. The pore-space is shown in black and rock matrix in white.

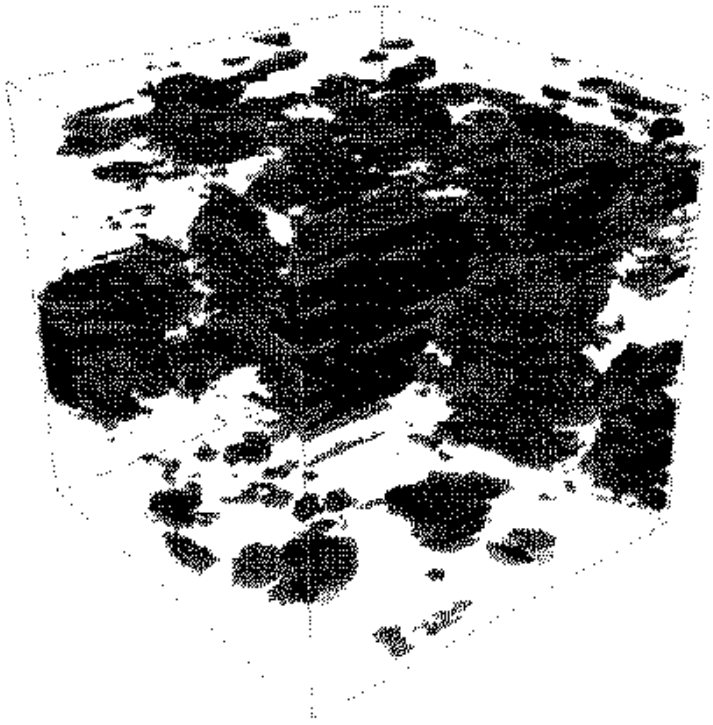

.

Figure 10: A roughly cubic sub-volume of 100x100x99 voxels from the same sandstone shown in the previous figure. The pore-space is shown in black, matrix is transparent and the pore-space boundary is gray.

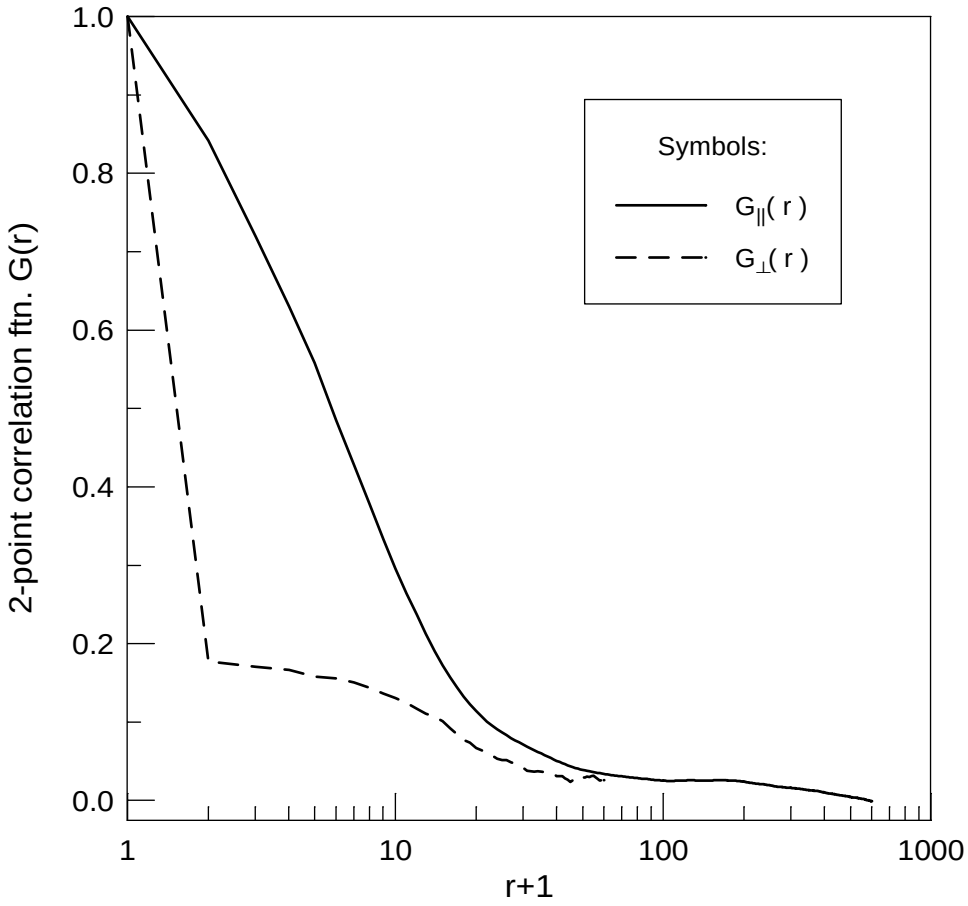

.

Figure 11: Two-point correlation functions for the sandstone specimen. $G_{\parallel}(r)$ and $G_{\perp}(r)$ are shown as the solid and dashed curves respectively. These functions are shown as functions of $r+1$ in order to plot the r-axis in logarithmic scale. Note the presence of several correlation-lengths in $G_{\parallel}$.

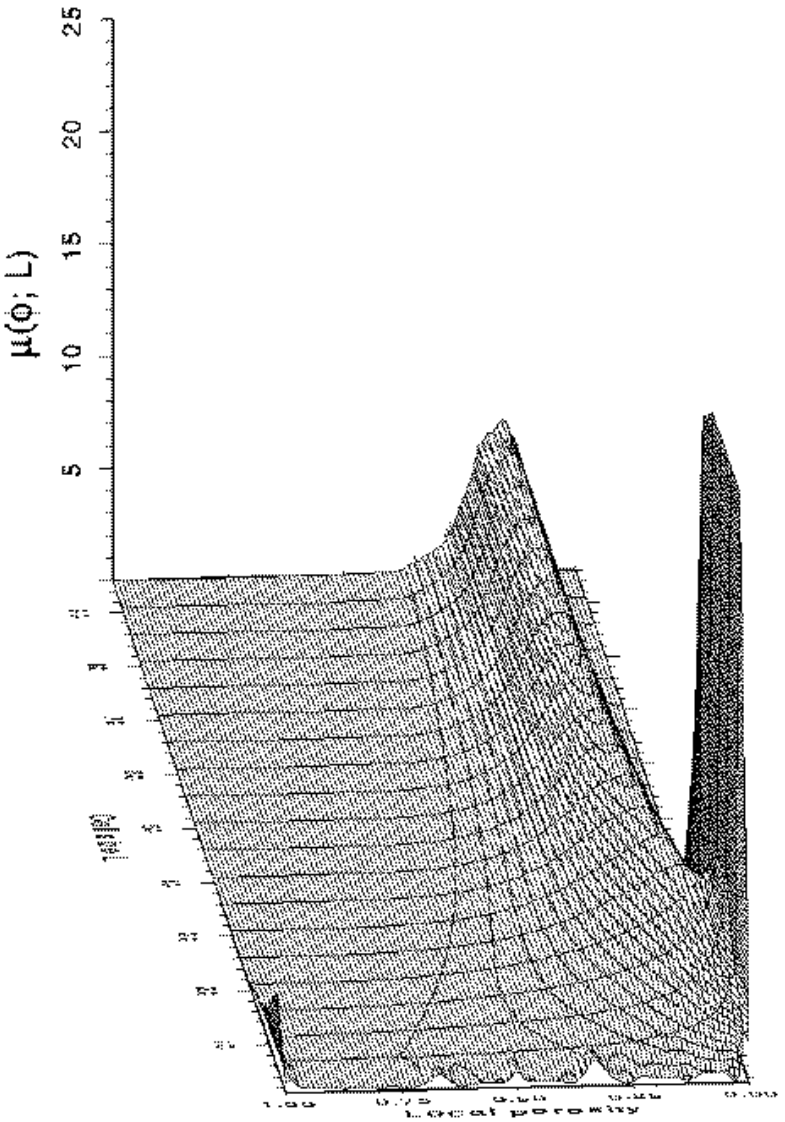

.

Figure 12: The family of three-dimensional LPDs $\mu_{3d}(\phi; L)$ for $L \in \{1, 2, \ldots, 96\}$ for Savonnier oolithic sandstone. The spikes at regular intervals for small L are not fluctuations, but rather a result of the anisotropy visible in Figure 10 and Figure 11.

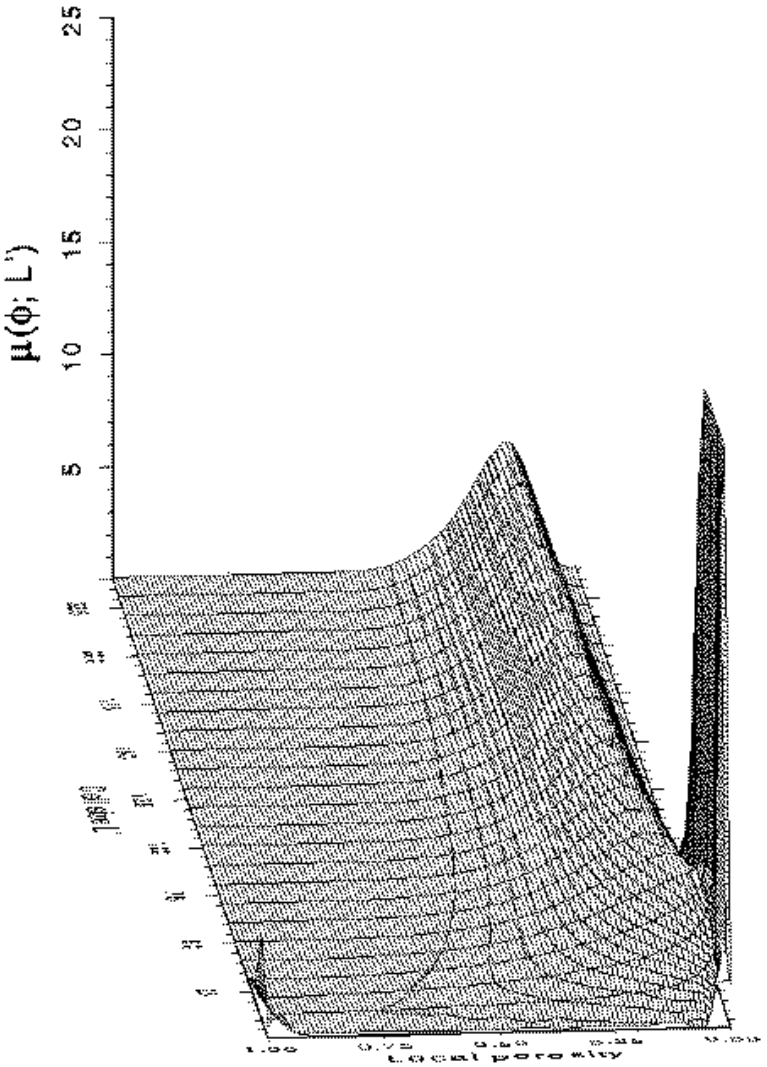

.

Figure 13: The family of two-dimensional LPDs $\mu_{2d}(\phi; L\ ')$ for $L^{'} \in \{1, 2, \ldots, 240\}$. Note that the distributions are much broader than those for the overlapping sphere model shown in Figure 3.

tained using $G_{\|}$ in (3). The poor agreement for $d = 3$ is to be expected, since $G_{\|} \neq G_{\perp}$, as seen in Figure 11. Hence, we cannot make an independent determination of the three-dimensional variance from the two-dimensional data, and are unable to construct the mapping $L^{'}(L)$ based on two-dimensional correlation functions.

Nevertheless, a matching between two- and three-dimensional LPDs can be obtained based on $\Delta(L, L^{'})$ as discussed above. The results of the Δ-matching procedure are shown in Figure 15 for a selection of $(L, L^{'})$-pairs indicated in the figure. The agreement is of similar quality as that for the overlapping sphere model.

7 Conclusion

The present paper has investigated the dimensional dependence of local porosity distributions, which formalize the idea of length-scale dependent spatial averaging (coarse-graining). We have presented the first determinations of LPDs for real porous media. We have shown that in general, in the limit of large measurement cells(averaging regions), the two- and three-dimensional LPDs can be mapped onto each other by a rescaling of lengths $L^{'}(L)$. This result was based on the central limit theorem and the concept of stationarity. We have found that the mapping $L^{'}(L)$ extends below the asymptotic regime to much smaller length-scales. This result is important for both practical applications and because it agrees with the possibility of intermediate limit laws for LPDs based on generalizations of the central limit theorem[3].

An equally important result of this paper is the finding that the mapping $L^{'}(L)$ can be determined from purely two-dimensional measurements. However, this result is restricted to homogeneous isotropic media.

We illustrated our results with three examples. For the percolation model, the analytical form of the mapping $L^{'}(L)$ between two- and three-dimensional LPDs is exactly known, and the agreement between mapped distributions becomes perfect. For the homogeneous isotropic overlapping sphere model, the agreement between mapped distributions is satisfactory for measurement cells of side $L \geq \xi$ and improves with increasing L. The mapping $L^{'}(L)$ can be successfully determined from two-dimensional observations alone for this medium. The three-dimensional pore-space reconstruction for the Savonnier

.

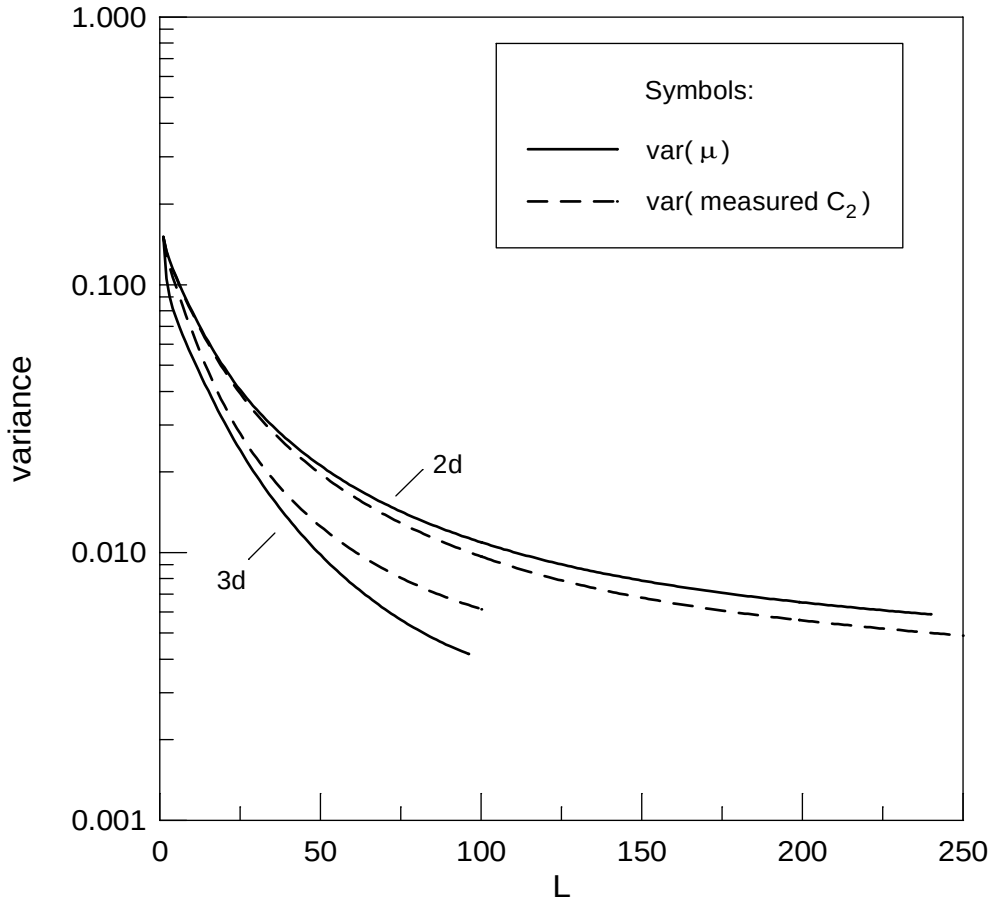

Figure 14: Two- and three-dimensional local porosity variances for the Savonnier oolithic sandstone. The solid curves are variances determined directly from the distributions and the dashed curves are variances computed from (3) using the $G_{\|}(r)$.

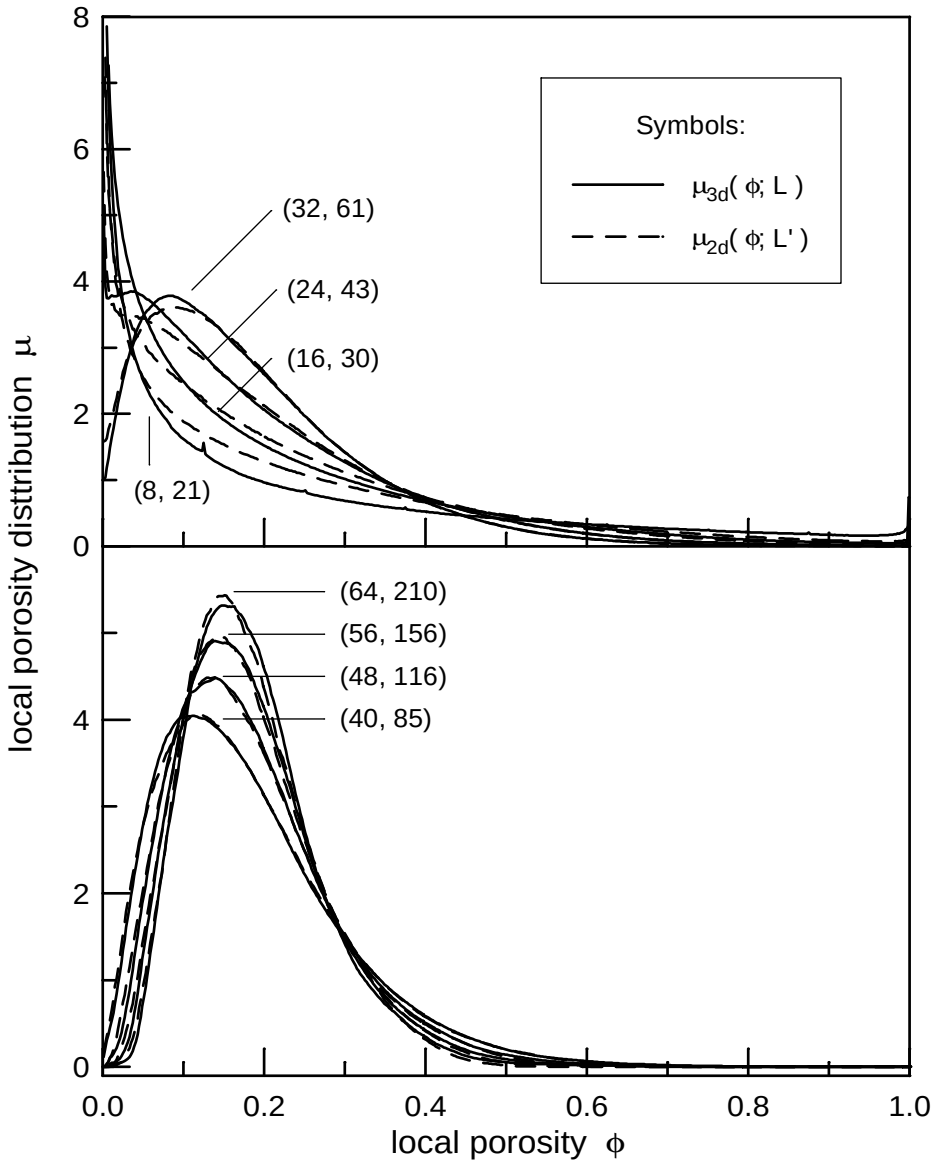

.

Figure 15: $\Delta(L, L^{'})$-matched two- and three-dimensional LPDs for the Savonnier oolithic sandstone for a selection of $(L, L^{'})$-pairs indicated in the figure. The two- and three-dimensional distributions are shown as dashed and solid curves, respectively. The spikes in Figure 12a are seen here in $\mu_{3d}(\phi; 8)$ at $\phi = 1/8, 2/8$ and $3/8$.

oolithic sandstone specimen is clearly anisotropic and shows large-scale heterogeneities. The anisotropy of the reconstructed pore-space does not allow one to construct the mapping $L^{'}(L)$ from two-dimensional observations. Nevertheless, the mapped curves from two- and three-dimensional measurements again show good agreement.

8 Acknowledgements

We wish to thank C. Ostertag-Henning and Prof. Dr. R. Koch from the Dept. of Palaeontology at the Univ. of Erlangen for generously providing us with a three-dimensional pore-space reconstruction of a Savonnier oolithic sandstone specimen. We also wish to thank Prof. Bjarne Nøst of the Dept. of Physics at the Univ. of Oslo, and Dr. U. Mann and Prof. Dr. D. H. Welte at the Forschungszentrum Jülich for discussion. Two of us(R.H and E.H) wish to thank the Norges Forskningsråd for partial financial support.

References

[1] R Landauer, "Electrical conductivity in inhomogeneous media", in *Electrical Transport and Optical Properties of Inhomogeneous materials*(J. Garland and D. Tanner, eds.), (New York), p. 2, American Institute of Physics, 1978.

[2] W. Mochan and R. Barrera(eds.), *ETOPIM 3, Proceedings of the Third International Conference on Electrical Transport and Optical Properties of Inhomogeneous Media*, vol. Physica A 207. Amsterdam: North Holland, 1994.

[3] R. Hilfer, "Transport and Relaxation in Porous Media", *Adv. Chem. Phys.*, vol. XCII, p. 299, 1996, in print.

[4] M. Sahimi, "Flow phemomena in rocks: From continuum models fractals, percolation, celullar automata and simulated annealing", *Rev. Mod. Phys.*, vol. 65, p. 1393, 1993.

[5] J. Lafait and D. Tanner(eds.), *ETOPIM 2, Proceedings of the Second International Conference on Electrical and Optical Properties of Inhomogeneous Media*, vol. Physica A 157. Amsterdam: North Holland, 1989.

[6] P.Debye and A. Bueche, "Scattering by an inhomogeneous solid", *L. Appl. Phys.*, vol. 20, p. 518, 1949

[7] P.Debye and A. Bueche, "Scattering by an inhomogeneous solid II: The correlation function and its application", *L. Appl. Phys.*, vol. 28, p. 679, 1957

[8] H. Weissberg, "Effective diffusion coefficient in porous media", *J. Appl. Phys.*, vol. 34, p. 2636, 1963.

[9] S. Torquato and G. Stell, "Microstructure of Two Phase Random Media I: The n-Point Probability Functions", *J. Chem. Phys.*, vol. 77, p. 2071, 1982.

[10] S. Torquato and G. Stell, "Microstructure of Two Phase Random Media II: The Mayer-Montroll and Kirkwood-Salsburg Heirarchies", *J. Chem. Phys.*, vol. 78, p. 3262, 1983.

[11] P. Rikvold and G. Stell, "Porosity and specific surface for impenetrable-sphere models of two-phase random media", *J. Chem. Phys.*, vol. 82, p. 1014, 1985.

[12] P. Rikvold and G. Stell, "D-dimensional interpenetrable sphere models of random two-phase media: Microstructure and applications to chromotography", *J. Colloid and Interface Sci.*, vol. 108, p. 158, 1985.

[13] G. Stell and P. Rikvold, "Polydispersity in fluids and composites: Some theoretical results", *Int. J. Thermophysics*, vol. 7, p. 863, 1986.

[14] J. Berryman, "Measurement of spatial correlation functions using image processing techniques", *J. Appl. Phys.*, vol. 57, p. 2374, 1985

[15] J. Berryman and S. Blair, "Use of digital image analysis to estimate fluid permeability of porous media: Application of two-point correlation functions", *J. Appl. Phys.*, vol. 60, p. 1930, 1986

[16] R. Hilfer, "Geometric and dielectric charaterizations of porous media", *Phys. Rev. B*, vol. 44, p. 60, 1991.

[17] F.Boger, J. Feder, R. Hilfer, and T. Jøssang, "Microstructural sensitivity of local porosity distributions", *Physica A*, vol. 187, p. 55, 1992.

[18] R. Hilfer, "Local porosity theory for flow in porous media", *Phys. Rev. B*, vol. 45, p. 7115, 1992.

[19] R. Hilfer, B. Nøst, E. Haslund, T. Kautzsch, B. Virgin and B. D. Hansen, "Local porosity theory for the frequency dependent dielectric function of porous rocks and polymer blends", *Physica A*, vol. 207, p. 19, 1994.

[20] E.Haslund, B. D. Hansen, R. Hilfer, and B. Nøst, "Measurements of local porosities and dielectric dispersion for a water saturated porous medium", *J. Appl. Phys.*, vol. 76, p. 5473, 1994.

[21] E. O'Neill, *Introduction to Statistical Optics*, Reading: Addisons-Wesley, 1963.

[22] D. A. Coker, S. Torquato, "Extraction of morphological quantities from a digitized medium", *J. Appl. Phys.*, vol. 77, p. 6087, 1995.

[23] C. Ostertag-Henning, B. Virgin, T. Rage, R. Hilfer, R. Koch and U. Mann, "Messung dreidimensionaler lokaler Porositiätsverteilungen", 1995, unpublished.